



HAL
open science

On-demand reversible switching of the emission mode of individual semiconductor quantum emitters using plasmonic metasurfaces

Adam Olejniczak, Zuzanna Lawera, Mario Zapata-Herrera, Andrey Chuvilin, Pavel Samokhvalov, Igor Nabiev, Marek Grzelczak, Yury Rakovich, Victor Krivenkov

► To cite this version:

Adam Olejniczak, Zuzanna Lawera, Mario Zapata-Herrera, Andrey Chuvilin, Pavel Samokhvalov, et al.. On-demand reversible switching of the emission mode of individual semiconductor quantum emitters using plasmonic metasurfaces. *APL Photonics*, 2024, 9 (1), pp.016107. 10.1063/5.0170535 . hal-04450588

HAL Id: hal-04450588

<https://hal.science/hal-04450588>

Submitted on 10 Feb 2024

HAL is a multi-disciplinary open access archive for the deposit and dissemination of scientific research documents, whether they are published or not. The documents may come from teaching and research institutions in France or abroad, or from public or private research centers.












L'archive ouverte pluridisciplinaire **HAL**, est destinée au dépôt et à la diffusion de documents scientifiques de niveau recherche, publiés ou non, émanant des établissements d'enseignement et de recherche français ou étrangers, des laboratoires publics ou privés.



Distributed under a Creative Commons Attribution 4.0 International License

RESEARCH ARTICLE | JANUARY 10 2024

On-demand reversible switching of the emission mode of individual semiconductor quantum emitters using plasmonic metasurfaces

Adam Olejniczak ; Zuzanna Lawera ; Mario Zapata-Herrera ; Andrey Chuvilin ; Pavel Samokhvalov ; Igor Nabiev ; Marek Grzelczak ; Yury Rakovich  ; Victor Krivenkov  

 Check for updates

APL Photonics 9, 016107 (2024)

<https://doi.org/10.1063/5.0170535>




CrossMark



APL Photonics
Future Luminary Collection

[Read Now!](#)



On-demand reversible switching of the emission mode of individual semiconductor quantum emitters using plasmonic metasurfaces

Cite as: APL Photon. 9, 016107 (2024); doi: 10.1063/5.0170535

Submitted: 3 August 2023 • Accepted: 11 December 2023 •

Published Online: 10 January 2024



View Online



Export Citation



CrossMark

Adam Olejniczak,¹  Zuzanna Lawera,¹  Mario Zapata-Herrera,^{1,2}  Andrey Chuvilin,^{3,4} 
Pavel Samokhvalov,^{5,6}  Igor Nabiev,^{5,6,7}  Marek Grzelczak,^{1,2}  Yury Rakovich,^{1,2,3,8,a)} 
and Victor Krivenkov^{1,8,a)} 

AFFILIATIONS

¹ Centro de Física de Materiales (MPC, CSIC-UPV/EHU), Donostia-San Sebastián 20018, Spain

² Donostia International Physics Center (DIPC), Donostia-San Sebastián 20018, Spain

³ Ikerbasque, Basque Foundation for Science, Bilbao 48013, Spain

⁴ CIC NanoGUNE Consolider, Tolosa Hiribidea 76, Donostia-San Sebastián 20018, Spain

⁵ Life Improvement by Future Technologies (LIFT) Center, Skolkovo, 143025 Moscow, Russia

⁶ National Research Nuclear University MEPhI (Moscow Engineering Physics Institute), 115409 Moscow, Russia

⁷ Laboratoire de Recherche en Nanosciences, LRN-EA4682, Université de Reims Champagne-Ardenne, 51100 Reims, France

⁸ Polymers and Materials: Physics, Chemistry and Technology, Chemistry Faculty, University of the Basque Country (UPV/EHU), Donostia-San Sebastián 20018, Spain

^{a)} Authors to whom correspondence should be addressed: yury.rakovich@ehu.eus and victor.krivenkov@ehu.eus

ABSTRACT

The field of quantum technology has been rapidly expanding in the past decades, yielding numerous applications, such as quantum information, quantum communication, and quantum cybersecurity. At the core of these applications lies the quantum emitter (QE), a precisely controllable generator of either single photons or photon pairs. Semiconductor QEs, such as perovskite nanocrystals and semiconductor quantum dots, have shown much promise as emitters of pure single photons, with the potential for generating photon pairs when hybridized with plasmonic nanocavities. In this study, we have developed a system in which individual quantum emitters and their ensembles can be traced before, during, and after the interaction with an external plasmonic metasurface in a controllable way. Upon coupling the external plasmonic metasurface to the QE array, the individual QEs switch from the single-photon emission mode to the multiphoton emission mode. Remarkably, this method preserves the chemical structure and composition of the QEs, allowing them to revert to their initial state after decoupling from the plasmonic metasurface. This significantly expands the potential applications of semiconductor QEs in quantum technologies.

© 2024 Author(s). All article content, except where otherwise noted, is licensed under a Creative Commons Attribution (CC BY) license (<http://creativecommons.org/licenses/by/4.0/>). <https://doi.org/10.1063/5.0170535>

I. INTRODUCTION

The impacts of the second quantum revolution will extend across numerous sectors within the society, including healthcare, finance, defense, weather modeling, and cybersecurity.¹ They have given rise to advanced fields in quantum communication and computing, collectively referred to as quantum information, including

the transmission, storage, and processing of information using quantum systems. The basic unit of quantum information is the quantum bit (qubit), which is fundamentally different from the classical bit. The latest quantum information protocols rely on photon-based qubits. Quantum emitters (QEs), used as sources of light in quantum information, require specific single-photon emission statistics. Crucial traits of an optimal QE include a high

single-photon purity, indistinguishability, high operation rate, and high brightness.² Apart from single photons, some of the advanced quantum information protocols deal with quantum-entangled photon pairs.^{3,4} Therefore, controllable on-demand sources of photon pairs are also regarded as QEs.^{5,6}

Indistinguishable single photons and entangled photon pairs are routinely generated by parametric down-conversion.⁷ However, this nonlinear process yields a probabilistic quantity of photons, with zero and multiple photons also generated, and it lacks the capability for on-demand generation of single photons or photon pairs. Thus, it cannot be used to obtain QEs. This is the cause of recent efforts to designing QEs that are based on cold atoms or ions, superconducting circuits, and solid-state sources, including emitting vacancy centers in diamond and fluorescent nanocrystals.^{8,9} Solid-state QEs, among other QEs, offer an enhanced flexibility in terms of integration into optical logic circuits and interfacing with traditional silicon electronics. Semiconductor quantum dots (QDs) and perovskite nanocrystals (PNCs) are among the most promising types of solid-state nanocrystal QEs. Given their high photoluminescence (PL) quantum yield (QY), they can serve as on-demand sources of single photons, with the ability to generate photon pairs.^{10–12} The emission of a photon pair by a semiconductor QE occurs due to the cascade recombination of the excited biexciton state to the ground state via the single-exciton state. The photon pair emitted in this process can be quantum entangled.^{4,9,13–16} However, the low PL QY of the biexciton emission in semiconductor QEs strongly limits their use as the source of entangled photon pairs. Due to the strong Coulomb interaction of hot carriers (two holes and two electrons) forming the biexciton, the Auger-like recombination process in nanocrystals is very fast.¹⁷ Hence, the most likely mechanism of the biexciton-to-exciton transition is nonradiative relaxation, which considerably decreases the overall PL QY compared to the transition of a single exciton to the ground state.

The light-matter coupling of QEs with optical microcavities or plasmonic nanocavities can help overcome this constraint by employing the Purcell effect to enhance the PL QY of the biexciton-to-exciton transition.^{9,18,19} The Purcell effect also leads to an increase in the QE operating rate,²⁰ which determines a better indistinguishability of the emitted single photons and a high entanglement fidelity of the emitted photon pairs.^{15,21} For attaining the Purcell effect, two types of electromagnetic cavities can be used: optical microcavities (such as Fabry-Pérot cavities, photonic crystals, and Mie resonators) and plasmonic metal “nanocavities” (such as single nanoparticles, dimer antennas, nanopatch antennas, and metasurfaces). Optical microcavities offer high quality factors, but their mode volumes are always larger than the diffraction limit, which constrains the absolute values of light-matter coupling strength and the Purcell factor.^{22,23} In contrast, plasmonic nanocavities are metal nanostructures in which resonant oscillations of the electron density (known as localized surface plasmons) emerge from their interaction with light.²⁴ These oscillations allow a much better localization of the electromagnetic modes at the nanoscale even below the diffraction limit, leading to the maximum possible Purcell factor, up to two orders of magnitude higher compared to those of optical microcavities.²⁵ Therefore, a significant acceleration of radiative relaxation makes it possible to obtain highly efficient on-demand multiphoton emission from an individual semiconductor QE.^{26–28} Furthermore, plasmonic metasurfaces can be used instead of individual plasmonic

nanoparticles. As macroscale structures, metasurfaces are capable of light-matter coupling with macroscopic ensembles of emitters.^{29,30}

In photonic structures with QEs attached to plasmonic nanostructures, QEs with an increased biexciton PL QY are multiphoton emission sources and can no longer serve as single-photon sources.^{26–28} Our research presents an alternative solution to the common problem of choice between single-photon and multiphoton emissions of individual QEs. Here, we demonstrate the possibility of plasmon-induced reversible switching of individual semiconductor QEs from single-photon emission to multiphoton emission by controllable manipulation of the distance between the QEs and a plasmonic metasurface.

II. RESULTS

We used cesium lead-halide ($\text{CsPbBr}_{2.5}\text{I}_{0.5}$) PNCs synthesized using the modified supersaturated recrystallization technique as plasmon-controlled solid-state QEs.³¹ The size of the PNCs was about 15 nm [Fig. 1(a)]. Their maximum PL in a hexane solution under normal conditions was at a wavelength of 530 nm, with a full width at half maximum (FWHM) of 20 nm [Fig. 1(b)] and a PL QY of 25%. The corresponding PL decay kinetics is well fitted by a three-exponential function [Fig. 1(c)] with an amplitude-weighted average (AWA) lifetime of 11.5 ns. The QEs represented PNCs incorporated into a 15 nm thick poly(methyl methacrylate) (PMMA) film on the surface of a glass slide. The optical properties of the PNCs changed when they were embedded into the film: The PL peak was shifted to 520 nm and narrowed to an FWHM of 15 nm [Fig. 1(d)], and the PL lifetime was shortened to an average of 6.3 ns [Fig. 1(c)]. We can attribute these changes to partial loss of iodine ions by the PNCs during the film fabrication. This is due to the possibility of migration of iodine ions within the crystal structure of PNCs.³² During the film deposition procedure, some iodine ions can migrate to the PNC surface, where they undergo oxidation into volatile I_2 (iodine), causing irreversible changes in the PNC stoichiometry. This, in turn, leads to a blue shift and narrowing of the emission spectrum, making it more similar to that of the emission of pure CsPbBr_3 PNCs.^{31,32}

The initial step of each experiment included identifying individual PNCs [Fig. 1(e)] through the measurement of the second-order cross correlation function $g^{(2)}$. The single-QE behavior of the selected PNCs was considered proved if the central peak of the $g^{(2)}$ function of a single QE was below 50% of the side peaks [Fig. 1(f)].³³ In addition, we measured the PL intensity-time traces of these individual PNCs, which showed the PL blinking behavior typical of semiconductor nanocrystals [Fig. 1(g)].

Plasmonic metasurfaces were obtained using PVP-coated 75-nm silver nanocubes (SNCs) commercially available in the form of an ethanol solution from nanoComposix (USA). Their SEM images and optical properties are shown in Figs. S3(a) and S3(d). Initially, we used the deposition of SNCs directly onto the surface of the PNC-PMMA film by drop-casting the stock solution [Fig. S3(c)], as done in previous studies.^{26,28} For details, see Sec. 2.2 of the supplementary material. However, the total PNC PL intensity was significantly reduced after the treatment of PNCs with ethanol, and the addition of SNCs only slightly increased the PNC PL intensity, not restoring it to the initial value (Fig. S4). The drop in the PL intensity due to PNC deterioration in the presence of ethanol did not

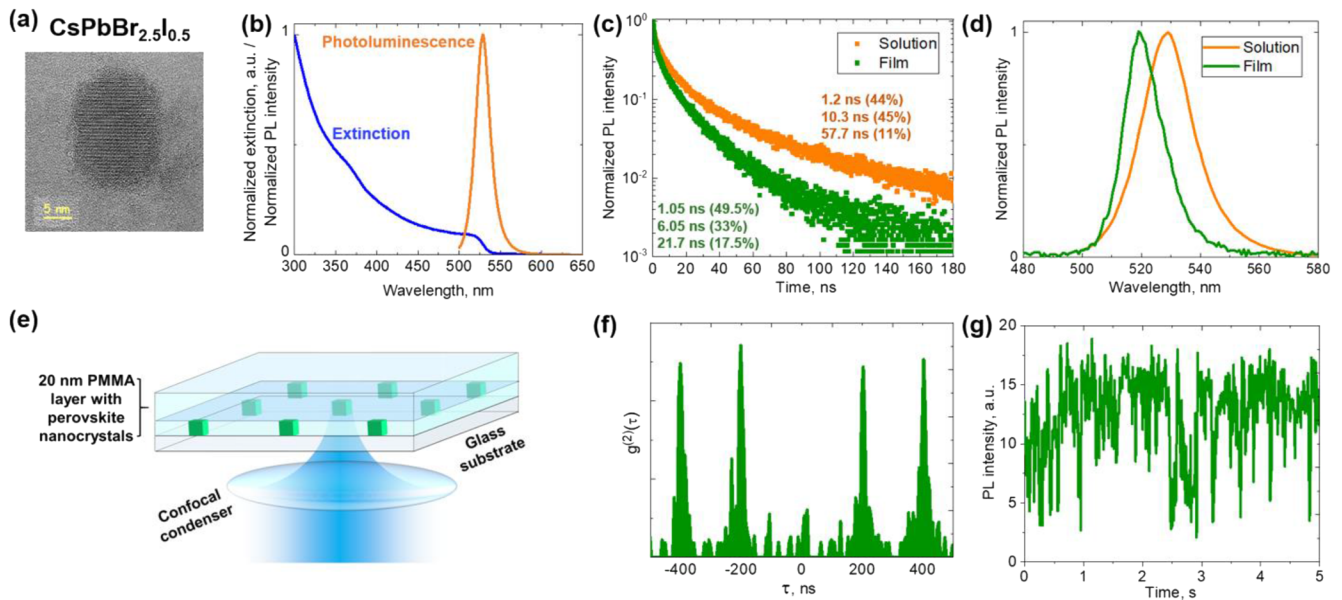


FIG. 1. Characteristics of the PNCs used. (a) TEM image of an individual PNC; (b) extinction and PL spectra of the hexane solution of PNCs; (c) PL decay kinetics for the hexane solution of PNCs (orange dots) and the PNC–PMMA thin film (green dots); (d) change in the PL spectrum of PNCs after transfer from the hexane solution to the thin PMMA film; (e) measurement geometry; (f) characteristic $g^{(2)}$ function of an individual PNC; and (g) characteristic PL intensity–time trace of an individual PNC.

allow us to discern the PL-enhancing effect of SNCs on the biexciton emission efficiency. Therefore, we changed the approach to the formation of the PNC–SNC hybrid system. To achieve a greater PL enhancement, we replaced the SNC deposition by drop-casting with mechanical merging of the thin PNC film and a curved glass surface (with a curvature radius of 50 cm) coated with SNCs [Fig. 2(a)]. Before the SNC deposition on the glass surface, the full width at half maximum (FWHM) of the extinction spectrum of the SNC solution was 110 nm, and the spectrum peak was at a wavelength of 508 nm [the orange line in Fig. S3(d)]. The FWHM of the extinction spectrum of the metasurface was 140 nm, and the peak position was at 515 nm [Fig. 2(b)]. The spectral shift and the spectrum broadening can be explained by the collective interaction of SNCs in the metasurface, which is corroborated numerically by calculating the extinction spectrum of an SNC array on a glass surface [red squares in Fig. S3(d)].

Before the formation of the plasmon–exciton hybrid system, we identified individual PNCs in the thin PNC–PMMA film using photon correlation spectroscopy [Fig. 2(c)]. In all experiments with individual QEs, we used at least five independent samples of each QE type. Then, we placed the SNC-covered curved plasmonic metasurface onto the PNC–PMMA sample. The geometry of the system was designed to ensure that a distance between the plasmonic metasurface and the surface of the PNC–PMMA film was maintained at less than 30 nm within the area of $\sim 0.2 \text{ mm}^2$. For more details, see Sec. 2.3 and Fig. S5 of the supplementary material. As shown in previous studies, this distance was adequate for facilitating efficient plasmon–exciton interactions.^{26,28} It should be noted that the lateral position of the PNCs in the image after the positioning of the plasmonic metasurface was not changed significantly, and we were able to find the same individual PNCs before and after the

interaction with the metasurface (Figs. S7 and S9). During the interaction of individual PNCs with the metasurface, the PNC PL decay time was considerably shortened [Fig. 2(i)]. The fastest component of the PL decay kinetics of the individual PNC before the interaction was ~ 800 – 1100 ps. Once coupled with the metasurface, it was reduced to 400 ps. This lifetime shortening was accompanied by a more than twofold PL intensity enhancement [Figs. 2(f)–2(h)]; therefore, we can attribute this to the acceleration of the radiative relaxation rate (Purcell effect) resulting from the coupling of the PNC emission transition with the bright scattering plasmon mode. During the plasmon–exciton interaction, the $g^{(2)}$ functions of the PNCs were altered, not corresponding to the single-photon emission behavior anymore [Fig. 2(c)]. An increase in the $g^{(2)}$ central peak to a value higher than 50% of that of the side peaks [Fig. 2(d)] evidenced an increase in the biexciton PL QY and the switching of the QEs to the multiphoton emission mode, as it was shown in our previous study.²⁸ After moving the plasmonic metasurface apart from the PNCs, we were able to study the same individual PNCs. We found that the $g^{(2)}$ function was almost entirely restored to the characteristic shape of the single-photon emission mode and the PL lifetime became close to the value measured before the establishment of the plasmon–exciton interaction [Figs. 2(e) and 2(i), respectively]. Thus, we showed $g^{(2)}$ reversibility for all samples in which the plasmon-induced multiphoton emission was enhanced.

It is worth noting that the utilization of the plasmonic metasurface instead of the deposition of the SNCs from a solution or employing techniques for obtaining a hybrid PNC–SNC system preserved the morphology, internal structure, and chemical composition of the PNCs. Therefore, we could restore the initial properties of the PNCs after the plasmon–exciton interaction ceased.

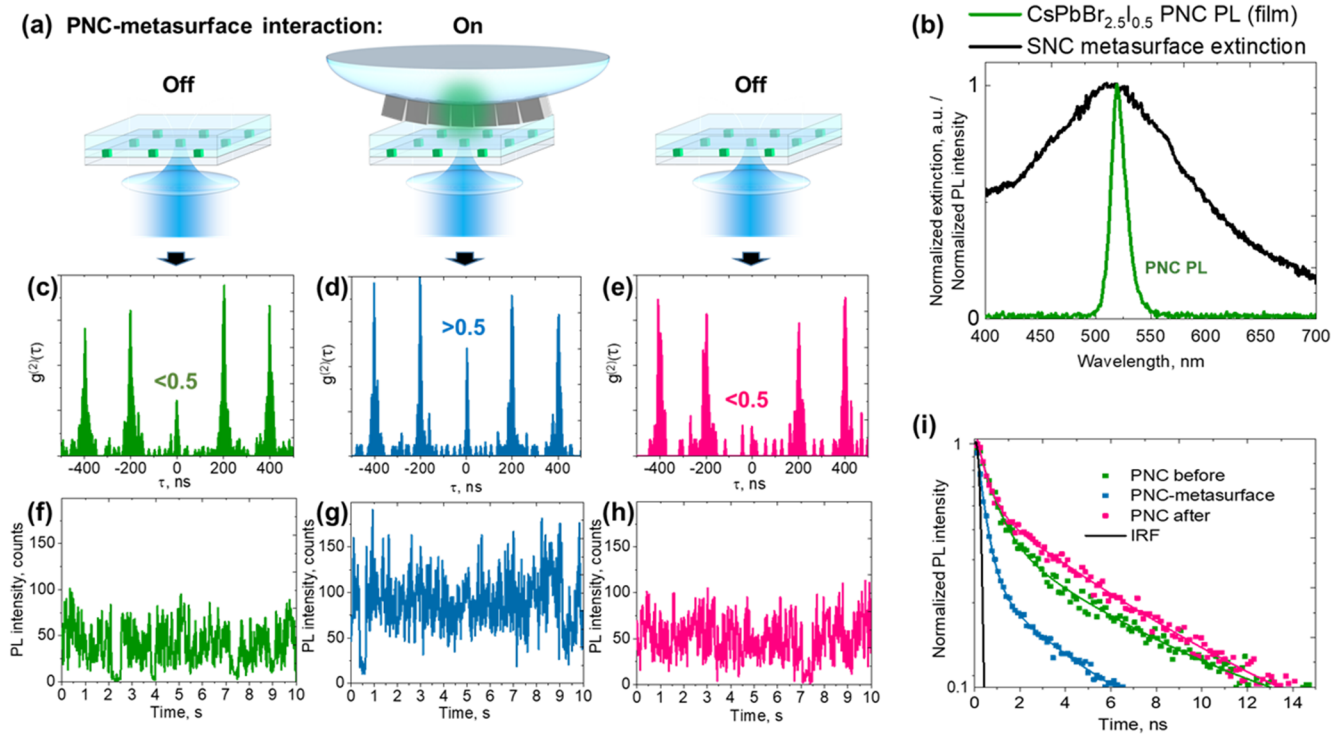


FIG. 2. Reversible effect of the interaction with the SNC plasmonic metasurface on the emission characteristics of individual PNCs. (a) Schematic representation of the experiment. (b) Extinction spectrum of the SNC plasmonic metasurface (black curve) and PNC emission spectrum (green curve). [(c)–(e)] $g^{(2)}$ functions of the same individual PNC before (c), during (d), and after (e) the interaction with the SNC plasmonic metasurface. [(f)–(h)] PL intensity traces of the same individual PNC before (f), during (g), and after (h) the interaction with the SNC plasmonic metasurface. (i) PL decay curves of the same individual PNC before (green), during (blue), and after (pink) the interaction with the SNC plasmonic metasurface.

The merging of the SNC plasmonic metasurface and PNCs increased the PL intensity of individual PNCs [Figs. 2(f)–2(h) and S6]. However, upon cessation of the plasmon–exciton interaction, the PL intensity was restored to its initial value, which indicates that the observed PL enhancement can be attributed to the coupling with the plasmonic metasurface.

The observed increase in the QE emission intensity may have resulted not only from the Purcell effect but also from the excitation enhancement caused by the SNCs.^{28,34} The essential condition for the excitation enhancement is a spectral overlap between the excitation band (peaking at 485 nm in our primary experiments) and the plasmon resonance of the SNCs. This condition was met in our experiments with the metasurface-based hybrid system [Fig. 2(b)].³⁴ To understand the possible influence of the excitation enhancement on the obtained results, we performed a control experiment using an excitation wavelength of 405 nm. In this experiment, the excitation of QEs was detuned from the plasmon resonance of the SNC plasmonic metasurface. Despite this change, we observed effects similar to those in the experiment with excitation at 485 nm (Fig. S7). Thus, the spectral overlap between the excitation band and the plasmon resonance had no effect on the results.

In all experiments on the interaction of SNC metasurfaces with PNCs, the total plasmon-induced enhancement factor of the

emission intensity of individual PNCs was between 2.2 and 7.5. In addition, the PL lifetime was decreased by a factor of 1.6 to 2.1 in these systems, although the expected factor of the radiative rate acceleration calculated using Eq. (S1) was in the range from 5 to 12. It is worth noting that the PL intensity enhancement was more pronounced for initially low-emitting PNCs compared to initially high-emitting PNCs (7.5-fold and 2.2-fold, respectively, as seen from Figs. S7 and 2). One possible explanation is that the increased radiative recombination rate had a more significant impact on the final PL QY of PNCs with an initially lower PL QY. Another contributing factor to the discrepancy in the PL intensity enhancement is the variation of the position of the QEs relative to individual SNCs in the metasurface. The calculated Purcell factor for the interaction of the SNCs with the QEs emitting at 520 nm (the spectral maximum of the PNC emission) located at a distance of 7.5 nm from the SNC corner was 8.3. However, the Purcell factor for the PNCs positioned close to the center of an SNC facet was only 1.3. Moreover, according to the simulated spatial distribution of the SNC plasmon modes [Fig. S3(d)], the area of the possible interaction with an SNC corner is much smaller than the area of interaction with a flat facet surface. Given the random distribution of PNCs relative to the SNCs, it was more likely for them to be located near the flat surface of the SNC facet rather than at the corner of SNC. For a large ensemble of PNCs

interacting with the SNC plasmonic metasurface, the total emission enhancement factor was about 2 (Fig. 3), which reflected the effects on both initially low-emitting and initially high-emitting PNCs at all possible positions relative to the SNC corners. For details on the numerical simulation of the interaction of individual QEs with the SNC, see Sec. 4 of the supplementary material.

In a second control experiment, we altered the overlap between the PNC emission spectrum and the plasmon band peak to explore whether the reversible interaction occurs under conditions outside the resonance. For this purpose, we prepared a metasurface using polyelectrolyte-assisted layer-by-layer assembly of SNCs on a curved glass surface.^{35,36} As a result of chemical degradation and etching of the SNC corners during deposition, the formed nanoparticle layer corresponded to a layer of nearly spherical plasmonic nanoparticles (PNPs) ~ 75 nm in size, exhibiting a plasmon resonance at a wavelength of 455 nm [Fig. S8(a)].³⁷ Unlike SNC-based metasurfaces, which had plasmon resonance at the same wavelength as PNC emission, the plasmon resonance peak of the PNP-based plasmonic metasurface was at a wavelength of 455 nm [Fig. S8(a)]. The spectral position of this plasmon resonance exclusively aligns with the excitation wavelength but not with the PNC emission spectrum. We employed the PNP-based metasurface to assess its impact on the emission of both an ensemble of PNCs [Fig. S8(b)] and individual PNCs (Fig. S9). As in the experiments with SNCs, we estimated the emission characteristics of the same PNCs before the deposition of the PNP-based metasurface, during the interaction of PNCs with the metasurface, and following the removal of the metasurface. The results showed only a drop of the PL intensity signal, without changes in other parameters studied. This confirmed that excitation enhancement did not play an important role in the designed technique.

To further explore the role of the Purcell effect in the designed technique, we investigated how the spectral overlap between the plasmon resonance and the QE emission affected the changes in the PL characteristics of other types of semiconductor QEs. Lead halide perovskites emitting in the red region of the optical spectrum are unstable because of the presence of iodine ions in the crystal structure.³⁸ Our attempt at incorporating red-emitting PNCs into the PMMA thin film using spin coating resulted in the destruction of the PNCs. To solve this problem, we used CdSe-based core/shell

QDs (QD560 and QD620 samples; see Sec. 2.1 of the supplementary material for details) whose emissions were not in resonance with the SNC metasurface plasmonic band, which weakened the Purcell effect [Figs. 4(a) and 4(b)]. Thus, using QD samples, we gradually reduced the potential Purcell effect by shifting the emission spectrum out of the resonance with the plasmonic band of the SNC-based metasurface. This allowed us to study how it affects the emission properties of QEs during the reversible plasmon–exciton interaction. In addition, we estimated the impact of the bare curved glass surface (not covered with SNCs) on the emission of individual QDs and found no changes in their emission properties. As a result, all the observed effects can be attributed to the interaction with the plasmonic metasurfaces.

In the case of the hybrid system containing QD560, the overlap between the QD emission spectrum and the plasmon resonance of the SNC plasmonic metasurface was smaller than in the case of PNCs [Fig. 4(b)]. In this experiment, the PL intensity was increased by 30% [Fig. 4(c)] and the PL lifetime significantly decreased [Fig. 4(e)]. The fastest PL decay component before the interaction was 3.2 ns, and it was reduced to 500 ps during the plasmon–exciton interaction. This considerable lifetime shortening was not accompanied by the corresponding strong enhancement of the emission intensity; therefore, we can conclude that it was related to the acceleration of both radiative and nonradiative relaxation rates of QDs. The simultaneous acceleration of both radiative and nonradiative processes results in a greater reduction in the PL lifetime compared to the scenario where only the radiative process is accelerated. Given that the PL intensity increased only by 30%, we can infer that the acceleration of the radiative relaxation (Purcell factor) for the interaction of QD560 with the metasurface was smaller than that for the interaction of PNCs. Indeed, as can be seen from Fig. 4(a), the calculated Purcell factor for the case when the QE is near the center of the SNC facet is only 0.7 at the wavelength corresponding to the QD560 emission maximum [Fig. 4(a)], which can explain the relatively small enhancement of the PL intensity. As in the case of PNCs, we observed switching of the emission of individual QDs in the QD560–metasurface hybrid structure to the multiphoton mode as a result of interaction with the SNCs and then back to the single-photon mode after the removal of the metasurface [Fig. 4(d)].

In contrast, plasmon–exciton interaction in the case of red-emitting QDs (QD620) led to a strong quenching of the PL of individual QDs, accompanied by a shortening of the PL lifetime [Figs. 4(f) and 4(g)]. The acceleration of the radiative relaxation rate induced by the coupling of the excitonic transitions with bright scattering plasmon modes (due to the Purcell effect) may have been weak or non-existent in the absence of resonance between QE emission and the plasmon band. Consequently, the observed reduction in the PL lifetime and emission intensity can be attributed either to the well-known effect of the metal-induced emission quenching or to the coupling with dark non-scattering plasmon modes. These interactions enhanced the nonradiative relaxation, which outweighed the relatively weakly accelerated radiative relaxation. The radiative rate acceleration calculated for the wavelength of 620 nm (corresponding to the QD620 emission maximum) was determined to be 0.2 when measured at the center of the SNC, indicating a possible fivefold decrease in the PL intensity. Notably, the observed quenching factor was smaller than the estimated value (approximately fourfold) due to the high Purcell factor at the SNC corners [6.2, as seen in Fig. 4(a)].

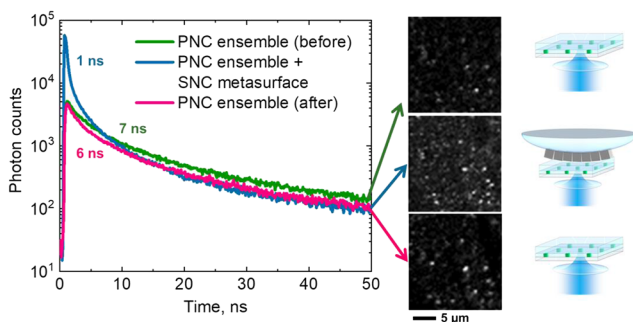


FIG. 3. PL signals collected from the ensemble of PNCs before the interaction with SNCs (green) with an AWA lifetime of 7 ns, during the interaction (blue) with an AWA lifetime of 1 ns, and after the removal of the SNC plasmonic metasurface (pink) with an AWA lifetime of 6 ns.

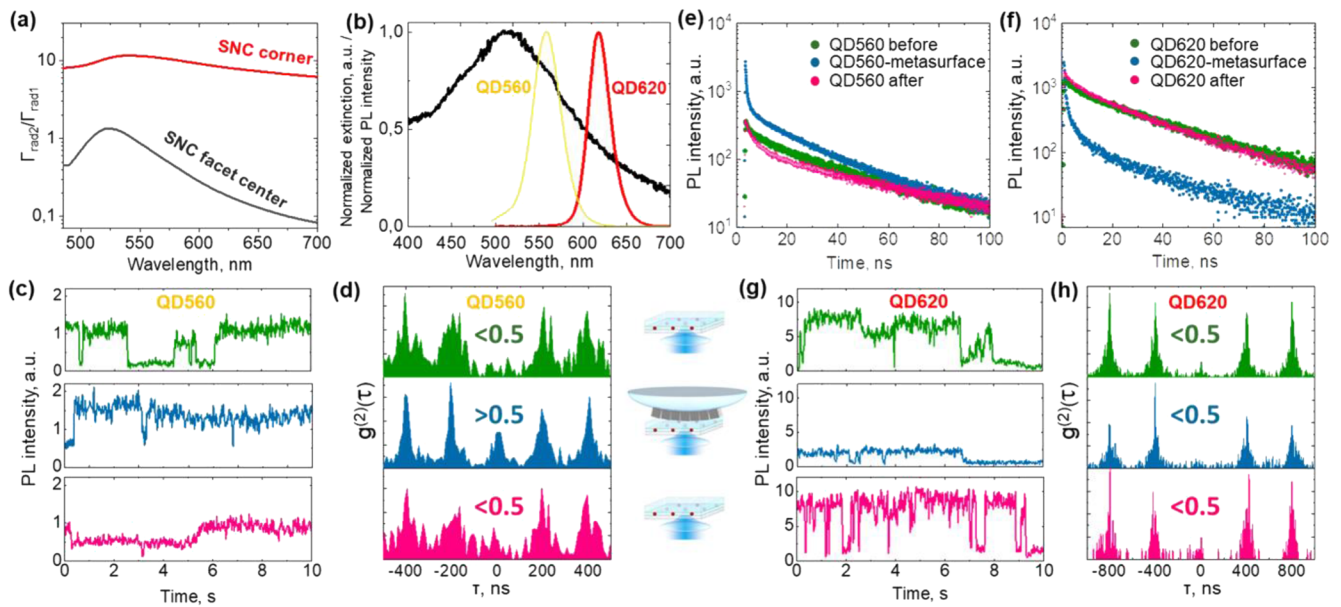


FIG. 4. Effect of the SNC plasmonic metasurface on the PL of individual QDs. (a) Calculated acceleration of the QE radiative rate 7.5 nm away from the center of the SNC facet (black line) and from the SNC corner (red line). (b) PL spectra of the QD560 (yellow line) and QD620 (red line) samples compared to the extinction of the SNC plasmonic metasurface (black line). (c) PL intensity trace and (d) second-order cross correlation function $g^{(2)}$ of the same single QD (QD560 sample) before the interaction with the SNC plasmonic metasurface (green), during the interaction (blue), and after the removal of the metasurface (pink). [(e) and (f)] PL decay kinetics of the same single QDs from the QD560 (e) and QD620 (f) samples before the interaction with the SNC plasmonic metasurface (green dots), during the interaction (blue dots), and after the removal of the metasurface (pink dots). (g) PL intensity trace and (h) the second-order cross correlation function $g^{(2)}$ of the same single QD (QD620 sample) before the interaction with the SNC plasmonic metasurface (green), during the interaction (blue), and after the removal of the metasurface (pink).

However, the contribution of the SNC corner area to the total area of the QE–metasurface interaction was relatively low. Moreover, we did not observe any effect of the metasurface on the $g^{(2)}$ function [Fig. 4(h)] of individual QDs. This supports the assumption that the increase in the radiative recombination rate (Purcell effect) led to the enhancement of biexciton emission and leveling of the exciton and biexciton PL QYs in the hybrid systems, characterized by a large overlap between the emission maximum and the plasmon resonance. Thus, we assume that the Purcell effect was the main factor ensuring the reversible switching between the single-photon and the enhanced multiphoton QE emission modes.

III. SUMMARY AND OUTLOOK

We have designed a plasmon–exciton hybrid system with a controlled Purcell factor based on disordered plasmonic metasurfaces and semiconductor QEs (semiconductor QDs and PNCs). This system allowed us to reversibly change (increase or decrease) the emission intensity and shorten the emission lifetime for ensembles of QEs of different types. Moreover, we achieved reversible switching of the emission mode from single-photon to multi-photon for individual QEs. Unlike previously published methods, the proposed technique does not require precise positioning of the AFM tip to the QE.^{39,40} Instead, we treated a whole array of QEs in the same way, and only the positioning of the objective lens was required for selecting the target QE. Further development of the new technique can include constructing an array of nano-patch antennas similar to

that developed by Dhawan *et al.*²⁷ but with a controlled gap distance. Moreover, precise positioning of QEs in hotspots of the plasmonic metasurface will enable an increase in the Purcell factor and, hence, a more efficient modulation of the emission mode. This concept can be used for the production of arrays of QEs with controlled emission characteristics, including the single-photon/multi-photon mode, emission rate, and intensity. The system proposed here has potential applications in the design of light-controlled QEs for quantum information applications and QLEDs with switchable emission characteristics controlled with the use of the light–matter coupling phenomenon.

IV. MATERIALS AND METHODS

A. Experimental setup

To measure PL signals and perform photon correlation spectroscopy, we used a MicroTime 200 inverted fluorescent microscope (PicoQuant, Germany) (Fig. S1). We used a water immersion $\times 60$ objective lens with NA = 1.2. Picosecond lasers emitting at 485 and 405 nm, each with a pulse duration of ~ 200 ps, were used as excitation sources. Photon correlation spectroscopy experiments were carried out using a setup with the Hanbury–Brown–Twiss geometry containing two avalanche photodiodes. The excitation line wavelength was separated using a long-pass optical filter with a cutting wavelength of 500 nm. Additionally, we used a 100- μm pinhole to purify the PL signal. Time-resolved PL measurements were performed in the time-correlated single-photon counting mode of

the MicroTime 200 system with only one avalanche photodetector. The system was used to measure both PL decay kinetics and PL intensity trace over a long time period.

B. Synthesis of CsPbBr_{2.5}I_{0.5} perovskite nanocrystals

All the reagents for the synthesis of CsPbBr_{2.5}I_{0.5} perovskite nanocrystals (PNCs) were purchased from Sigma-Aldrich and were used as received without further purification. First, 20 mg of CsBr, 26 mg of PbBr₂, and 11 mg of PbI₂ were dissolved in 2.235 ml of dimethylformamide (DMF). 223 μ l of oleic acid (OA) and 112 μ l of oleylamine (OAm) were added to stabilize the precursor solution. Then, 20 μ l of the precursor solution was quickly added into 2 ml of toluene under vigorous stirring at 2000 rpm. Immediately after the formation of a green colored solution, it was transfused to 10 ml of n-hexane. The optical density of the final PNC solution at the first exciton peak was 0.1. All the above-mentioned operations were carried out under normal conditions.

C. Synthesis of quantum dots

CdSe/ZnS/CdS/ZnS core/multishell quantum dots (QD560 sample) were synthesized according to the procedure described in our earlier study.²⁸ The method for synthesizing CdSe/CdS QDs (QD620 sample) is based on the method described by Chen *et al.*⁴¹ See Sec. 2.1 of the supplementary material for more details.

D. Preparation of quantum emitters in poly(methyl methacrylate) film samples

Earlier, we reported that the PL enhancement was achieved when the distance between QDs and plasmonic nanoparticles was between 10 and 20 nm.^{28,42} Therefore, in this study, we prepared QD–PNC arrays in poly(methyl methacrylate) (PMMA) films with a total thickness of \sim 15 nm. The thin films were deposited by the spin-coating method using a Model KW-4A Spin Coater at 1000 rpm for 60 s for each layer. First, the PMMA layer was deposited on a previously cleaned glass substrate using 70 μ l of 0.5 wt. % PMMA (120 000 Da). Then, the QDs (or PNCs) were deposited onto the PMMA surface from a hexane solution with a molar concentration of about 10^{-6} M. The second PMMA layer was deposited in the same way as the first one.

E. Preparation of the perovskite nanocrystal samples covered with a silver plasmonic metasurface

We used an ethanolic solution of silver nanocubes ([Ag⁰] = 0.6 mM) coated with a 3-nm layer of polyvinylpyrrolidone purchased from nanoComposix (USA). For the formation of plasmonic metasurfaces directly on the surface of the PNC–PMMA thin films, we applied 2 μ l of the SNC solution onto the PNC–PMMA structures [Fig. S3(b)]. For “dry” reversible deposition of the SNC metasurface onto the QE–PMMA thin films, we used a 2.5-cm round curved glass surface with a curvature radius of 50 cm. Before the deposition, 2 μ l of the stock solution of SNCs was dropped into the center of the curved glass surface and left until ethanol was evaporated and an array of SNCs was formed on the surface.

In order to change the plasmon resonance spectral position, the SNCs were attached to the curved glass surface using a different deposition method. A control sample prepared by the

polyelectrolyte-assisted layer-by-layer assembly method was found to have a different absorption spectrum compared to the drop-casting deposition.^{35,36} First, the curved glass surface was washed with an alkaline cleaning solution and sonicated in water and then in ethanol. The clean substrate was then immersed in a freshly prepared poly(diallyldimethylammonium chloride) solution purchased from Sigma-Aldrich (1 mg/ml in 0.5M NaCl) for 20 min and rinsed with Mili-Q water. Then, the curved glass was immersed for 1 h in the SNC solution. The substrate was rinsed with Mili-Q water and dried under argon flow.

F. Numerical calculations

All numerical simulations in this study were performed by the finite element method (FEM), using the COMSOL Multiphysics commercial software. The Radio Frequency Module of COMSOL was used to solve the Maxwell equations in the frequency domain in conjunction with proper boundary conditions. The optical constants of the SNCs were taken from the study by Johnson and Christy.⁴³ The refractive index of SiO₂ was assumed to be 1.45. See Sec. 4 of the supplementary material for more details.

SUPPLEMENTARY MATERIAL

See the supplementary material for details about the experimental setup, nanocrystal synthesis and characterization, thin-film sample preparation, deposition of SNCs onto the surface of the PNC–PMMA film, and related experimental results; the description of the preparation and use of the nanocrystal-coated curved glass surface; the results of photoluminescence and photon correlation spectroscopies at an excitation wavelength of 405 nm using PNPs and SNCs and at an excitation wavelength of 485 nm using SNCs; and details of the calculation of the Purcell factor.

ACKNOWLEDGMENTS

The study was funded by the European Union’s Horizon 2020 research and innovation program under the Marie Skłodowska-Curie, Grant Agreement No. 101025664 (QESPEM). Y.R. and V.K. acknowledge the support by MCIN and by the European Union NextGenerationEU/PRTR-C17.I1, as well as by IKUR Strategy under the collaboration agreement between Ikerbasque Foundation and Material Physics Center on behalf of the Department of Education of the Basque Government. Y.R. acknowledges the financial support from Grant No. TED2021-129457B-I00 funded by MCIN/AEI/10.13039/501100011033 and the European Union NextGenerationEU/PRTR and from the Department of Education of the Basque Government under Project Ref. IT1526-22. The part of the study related to the synthesis of semiconductor quantum dots was supported by the Russian Science Foundation (RSF), Grant No. 21-79-30048. Y.R. and A.O. also acknowledge the support from the Office of Naval Research Global (Award No. N62909-22-1-2031). M.G. and Y.R. acknowledge the financial support from Gipuzkoa Quantum (Quan 22) funded by Gipuzkoa Provincial Council. I.N. acknowledges the support from the French National Research Agency ANR, Grant No. ANR-20-CE19-009-02, and from the Université de Reims Champagne-Ardenne.

AUTHOR DECLARATIONS

Conflict of Interest

The authors have no conflicts to disclose.

Author Contributions

Adam Olejniczak: Data curation (equal); Formal analysis (equal); Investigation (equal); Methodology (equal); Software (equal); Validation (equal); Visualization (equal); Writing – review & editing (equal). **Zuzanna Lawera:** Investigation (equal); Methodology (equal); Writing – review & editing (equal). **Mario Zapata-Herrera:** Formal analysis (supporting); Software (equal). **Andrey Chuvin:** Investigation (equal); Resources (supporting). **Pavel Samokhvalov:** Investigation (equal); Writing – review & editing (equal). **Igor Nabiev:** Resources (supporting); Supervision (supporting); Writing – review & editing (lead). **Marek Grzelczak:** Methodology (supporting); Resources (supporting); Supervision (supporting). **Yury Rakovich:** Funding acquisition (lead); Methodology (equal); Project administration (lead); Resources (lead); Supervision (equal); Writing – review & editing (lead). **Victor Krivenkov:** Conceptualization (lead); Data curation (equal); Formal analysis (equal); Funding acquisition (equal); Investigation (equal); Methodology (equal); Project administration (equal); Software (equal); Supervision (equal); Validation (equal); Visualization (lead); Writing – original draft (lead); Writing – review & editing (lead).

DATA AVAILABILITY

The data that support the findings of this study are available from the corresponding author upon reasonable request.

REFERENCES

- 1 A. Acín, I. Bloch, H. Buhrman, T. Calarco, C. Eichler, J. Eisert, D. Esteve, N. Gisin, S. J. Glaser, F. Jelezko, S. Kuhr, M. Lewenstein, M. F. Riedel, P. O. Schmidt, R. Thew, A. Wallraff, I. Walmsley, and F. K. Wilhelm, “The quantum technologies roadmap: A European community view,” *New J. Phys.* **20**(8), 080201 (2018).
- 2 P. Senellart, G. Solomon, and A. White, “High-performance semiconductor quantum-dot single-photon sources,” *Nat. Nanotechnol.* **12**(11), 1026–1039 (2017).
- 3 C. Monroe, “Quantum information processing with atoms and photons,” *Nature* **416**(6877), 238–246 (2002).
- 4 F. Basso Basset, M. Valeri, E. Rocca, V. Muredda, D. Poderini, J. Neuwirth, N. Spagnolo, M. B. Rota, G. Carvacho, F. Sciarrino, and R. Trotta, “Quantum key distribution with entangled photons generated on demand by a quantum dot,” *Sci. Adv.* **7**(12), eabe6379 (2021).
- 5 F. Basso Basset, F. Salusti, L. Schweickert, M. B. Rota, D. Tedeschi, S. F. Covre da Silva, E. Rocca, V. Zwiller, K. D. Jöns, A. Rastelli, and R. Trotta, “Quantum teleportation with imperfect quantum dots,” *npj Quantum Inf.* **7**(1), 7–9 (2021).
- 6 M. Reindl, K. D. Jöns, D. Huber, C. Schimpf, Y. Huo, V. Zwiller, A. Rastelli, and R. Trotta, “Phonon-assisted two-photon interference from remote quantum emitters,” *Nano Lett.* **17**(7), 4090–4095 (2017).
- 7 A. Orioux, M. A. M. Versteegh, K. D. Jöns, and S. Ducci, “Semiconductor devices for entangled photon pair generation: A review,” *Rep. Prog. Phys.* **80**(7), 076001 (2017).
- 8 M. D. Eisaman, J. Fan, A. Migdall, and S. V. Polyakov, “Invited review article: Single-photon sources and detectors,” *Rev. Sci. Instrum.* **82**(7), 071101 (2011).
- 9 I. Aharonovich, D. Englund, and M. Toth, “Solid-state single-photon emitters,” *Nat. Photonics* **10**(10), 631–641 (2016).
- 10 P. Linkov, P. Samokhvalov, K. Vokhmintsev, M. Zvaigzne, V. A. Krivenkov, and I. Nabiev, “Optical properties of quantum dots with a core-multishell structure,” *JETP Lett.* **109**(2), 112–115 (2019).
- 11 F. Liu, Y. Zhang, C. Ding, S. Kobayashi, T. Izuishi, N. Nakazawa, T. Toyoda, T. Ohta, S. Hayase, T. Minemoto, K. Yoshino, S. Dai, and Q. Shen, “Highly luminescent phase-stable CsPbI₃ perovskite quantum dots achieving near 100% absolute photoluminescence quantum yield,” *ACS Nano* **11**(10), 10373–10383 (2017).
- 12 C. Zhu, M. Marczak, L. Feld, S. C. Boehme, C. Bernasconi, A. Moskalenko, I. Cherniukh, D. Dirin, M. I. Bodnarchuk, M. V. Kovalenko, and G. Rainò, “Room-temperature, highly pure single-photon sources from all-inorganic lead halide perovskite quantum dots,” *Nano Lett.* **22**, 3751 (2022).
- 13 M. Müller, S. Bounouar, K. D. Jöns, M. Glässl, and P. Michler, “On-demand generation of indistinguishable polarization-entangled photon pairs,” *Nat. Photonics* **8**(3), 224–228 (2014).
- 14 H. Utzat, W. Sun, A. E. K. Kaplan, F. Krieg, M. Ginterseder, B. Spokoyny, N. D. Klein, K. E. Shulenberg, C. F. Perkinson, M. V. Kovalenko, and M. G. Bawendi, “Coherent single-photon emission from colloidal lead halide perovskite quantum dots,” *Science* **363**(6431), 1068 (2019).
- 15 C. Schimpf, M. Reindl, F. Basso Basset, K. D. Jöns, R. Trotta, and A. Rastelli, “Quantum dots as potential sources of strongly entangled photons: Perspectives and challenges for applications in quantum networks,” *Appl. Phys. Lett.* **118**(10), 100502 (2021).
- 16 D. Huber, M. Reindl, J. Aberl, A. Rastelli, and R. Trotta, “Semiconductor quantum dots as an ideal source of polarization-entangled photon pairs on-demand: A review,” *J. Opt.* **20**(7), 073002 (2018).
- 17 Y.-S. Park, W. K. Bae, J. M. Pietryga, and V. I. Klimov, “Auger recombination of biexcitons and negative and positive trions in individual quantum dots,” *ACS Nano* **8**(7), 7288–7296 (2014).
- 18 S. Ates, S. M. Ulrich *et al.*, “Post-selected indistinguishable photons from the resonance fluorescence of a single quantum dot in a microcavity,” *Phys. Rev. Lett.* **103**(16), 167402 (2009).
- 19 T. B. Hoang, G. M. Akselrod, and M. H. Mikkelsen, “Ultrafast room-temperature single photon emission from quantum dots coupled to plasmonic nanocavities,” *Nano Lett.* **16**(1), 270–275 (2016).
- 20 V. S. C. Manga Rao and S. Hughes, “Single quantum-dot Purcell factor and β factor in a photonic crystal waveguide,” *Phys. Rev. B* **75**(20), 205437 (2007).
- 21 A. Saxena, Y. Chen, A. Ryou, C. G. Sevilla, P. Xu, and A. Majumdar, “Improving indistinguishability of single photons from colloidal quantum dots using nanocavities,” *ACS Photonics* **6**(12), 3166–3173 (2019).
- 22 H. Kaupp, T. Hümmer, M. Mader, B. Schleder, J. Benedikter, P. Haeusser, H. C. Chang, H. Fedder, T. W. Hänsch, and D. Hunger, “Purcell-enhanced single-photon emission from nitrogen-vacancy centers coupled to a tunable microcavity,” *Phys. Rev. Appl.* **6**(5), 054010 (2016).
- 23 T. Vogl, R. Lecamwasam, B. C. Buchler, Y. Lu, and P. K. Lam, “Compact cavity-enhanced single-photon generation with hexagonal boron nitride,” *ACS Photonics* **6**(8), 1955–1962 (2019).
- 24 J. J. Mock, M. Barbic, D. R. Smith, D. A. Schultz, and S. Schultz, “Shape effects in plasmon resonance of individual colloidal silver nanoparticles,” *J. Chem. Phys.* **116**(15), 6755 (2002).
- 25 S. I. Bozhevolnyi and J. B. Khurgin, “Fundamental limitations in spontaneous emission rate of single-photon sources,” *Optica* **3**(12), 1418 (2016).
- 26 V. Krivenkov, S. Goncharov, P. Samokhvalov, A. Sánchez-Iglesias, M. Grzelczak, I. Nabiev, and Y. Rakovich, “Enhancement of biexciton emission due to long-range interaction of single quantum dots and gold nanorods in a thin-film hybrid nanostructure,” *J. Phys. Chem. Lett.* **10**, 481–486 (2019).
- 27 A. R. Dhawan, C. Belacel, J. U. Esparza-Villa, M. Nasilowski, Z. Wang, C. Schwob, J. P. Hugonin, L. Coolen, B. Dubertret, P. Senellart, and A. Maitre, “Extreme multiexciton emission from deterministically assembled single-emitter subwavelength plasmonic patch antennas,” *Light Sci. Appl.* **9**(1), 33 (2020).
- 28 V. Krivenkov, D. Dyagileva, P. Samokhvalov, I. Nabiev, and Y. Rakovich, “Effect of spectral overlap and separation distance on exciton and biexciton quantum yields and radiative and nonradiative recombination rates in quantum dots near plasmon nanoparticles,” *Ann. Phys.* **532**(8), 2000236 (2020).
- 29 A. J. Traverso, J. Huang, T. Peyronel, G. Yang, T. G. Tiecke, and M. H. Mikkelsen, “Low-loss, centimeter-scale plasmonic metasurface for ultrafast optoelectronics,” *Optica* **8**(2), 202–207 (2021).

- ³⁰D. R. Dadadzhyanov, I. A. Gladskikh, M. A. Baranov, T. A. Vartanyan, and A. Karabchevsky, "Self-organized plasmonic metasurfaces: The role of the Purcell effect in metal-enhanced chemiluminescence (MEC)," *Sens. Actuators, B* **333**, 129453 (2021).
- ³¹X. Li, Y. Wu, S. Zhang, B. Cai, Y. Gu, J. Song, and H. Zeng, "CsPbX₃ quantum dots for lighting and displays: Room-temperature synthesis, photoluminescence superiorities, underlying origins and white light-emitting diodes," *Adv. Funct. Mater.* **26**(15), 2435–2445 (2016).
- ³²H. Zhang, X. Fu, Y. Tang, H. Wang, C. Zhang, W. W. Yu, X. Wang, Y. Zhang, and M. Xiao, "Phase segregation due to ion migration in all-inorganic mixed-halide perovskite nanocrystals," *Nat. Commun.* **10**(1), 1088 (2019).
- ³³B. D. Mangum, Y. Ghosh, J. A. Hollingsworth, and H. Htoon, "Disentangling the effects of clustering and multi-exciton emission in second-order photon correlation experiments," *Opt. Express* **21**(6), 7419–7426 (2013).
- ³⁴S. Dey, Y. Zhou, Y. Sun, J. A. Jenkins, D. Kriz, S. L. Suib, O. Chen, S. Zou, and J. Zhao, "Excitation wavelength dependent photon anti-bunching/bunching from single quantum dots near gold nanostructures," *Nanoscale* **10**(3), 1038–1046 (2018).
- ³⁵N. A. Kotov, I. Dekany, and J. H. Fendler, "Layer-by-layer self-assembly of polyelectrolyte-semiconductor nanoparticle composite films," *J. Phys. Chem.* **99**(35), 13065–13069 (1995).
- ³⁶S. Vial, I. Pastoriza-Santos, J. Pérez-Juste, and L. M. Liz-Marzán, "Plasmon coupling in layer-by-layer assembled gold nanorod films," *Langmuir* **23**(8), 4606–4611 (2007).
- ³⁷D. Paramelle, A. Sadovoy, S. Gorelik, P. Free, J. Hobley, and D. G. Fernig, "A rapid method to estimate the concentration of citrate capped silver nanoparticles from UV-visible light spectra," *Analyst* **139**(19), 4855–4861 (2014).
- ³⁸J. Hieulle, X. Wang, C. Stecker, D. Y. Son, L. Qiu, R. Ohmann, L. K. Ono, A. Mugarza, Y. Yan, and Y. Qi, "Unraveling the impact of halide mixing on perovskite stability," *J. Am. Chem. Soc.* **141**(8), 3515–3523 (2019).
- ³⁹H. Takata, H. Naiki, L. Wang, H. Fujiwara, K. Sasaki, N. Tamai, and S. Masuo, "Detailed observation of multiphoton emission enhancement from a single colloidal quantum dot using a silver-coated AFM tip," *Nano Lett.* **16**(9), 5770–5778 (2016).
- ⁴⁰S. Masuo, K. Kanetaka, R. Sato, and T. Teranishi, "Direct observation of multiphoton emission enhancement from a single quantum dot using AFM manipulation of a cubic gold nanoparticle," *ACS Photonics* **3**(1), 109–116 (2016).
- ⁴¹O. Chen, J. Zhao, V. P. Chauhan, J. Cui, C. Wong, D. K. Harris, H. Wei, H.-S. Han, D. Fukumura, R. K. Jain, and M. G. Bawendi, "Compact high-quality CdSe–CdS core–shell nanocrystals with narrow emission linewidths and suppressed blinking," *Nat. Mater.* **12**(5), 445–451 (2013).
- ⁴²V. Krivenkov, P. Samokhvalov, I. Nabiev, and Y. P. Rakovich, "Synergy of excitation enhancement and the Purcell effect for strong photoluminescence enhancement in a thin-film hybrid structure based on quantum dots and plasmon nanoparticles," *J. Phys. Chem. Lett.* **11**(19), 8018–8025 (2020).
- ⁴³P. B. Johnson and R. W. Christy, "Optical constants of the noble metals," *Phys. Rev. B* **6**(12), 4370–4379 (1972).